Broad lipid phase transitions in mammalian cell membranes measured by Laurdan fluorescence spectroscopy

Nicolas Färber [a,b], Christoph Westerhausen [a,b,c,*]

[a] Experimental Physics I, Institute of Physics, University of Augsburg, Universitätsstr. 1, 86159 Augsburg, Germany
[b] Physiology, Institute of Theoretical Medicine, University of Augsburg, Universitätsstraße 2, 86159 Augsburg, Germany
[c] Center for NanoScience (CeNS), Ludwig Maximilians Universität Munich, 80799 Munich, Germany

1. Introduction

Synthetic lipid double layers exhibit cooperative phase transitions causing their physical properties such as heat capacity, volume, area, thickness, stiffness, compressibility, adhesion forces, permeability and diffusion coefficient to depend on temperature, pressure, pH, electric field, salt concentration etc. in a non-linear way [1–9]. This correlation of phase state typically measured by differential scanning calorimetry (DSC) and membrane properties is well investigated for artificially created lipid membranes such as supported lipid bilayers and vesicles. If this concept also holds for biological cell membranes it is not only possible to predict their response to environmental changes but manipulating membrane functions such as permeability becomes possible simply by changing physical parameters like temperature or pH. However, in contrast to their synthetic analogues cell membranes consist of hundreds of distinct lipid and protein species without sharp transitions as protein addition and lipid mixing lead to transition peak broadening [10,11]. So far Heimburg et al. measured heat capacity profiles of *E. coli* bacteria by DSC and found an about 20 K broad phase transition some Kelvin below their growth temperature [3]. They could even demonstrate that bacteria cultured at lower temperature actively alter their membrane composition to shift the transition towards lower temperatures suggesting that the membrane phase state is connected to biological functions. However, we were not able to measure transitions in eukaryotic cell membranes by DSC. Reasons are suggested by the data presented below indicating that the transition regime is very broad and extends even below the freezing point of water. Therefore, we measure lipid order optically by analyzing the spectrum of the fluorescent dye Laurdan embedded in the membranes of HeLa, B35 and red blood cell ghosts. Laurdan is sensitive to the polarity and the relaxation dynamics of its environment and its fluorescence spectrum is red shifted from blue ($\lambda = 440$ nm) to green ($\lambda = 490$ nm) when the relaxation rate and the hydration level of the lipid membrane increase at the order-disorder-phase transition [12,13]. Furthermore, recent studies using magnetic

* Corresponding author at: Center for NanoScience (CeNS), Ludwig Maximilians Universität Munich, 80799 Munich, Germany.
E-mail address: christoph.westerhausen@gmail.com (C. Westerhausen).

resonance spectroscopy show a linear dependency of GP on lipid chain order [14]. By measuring the blue and green intensity of the Laurdan emission spectrum we calculate the Generalized polarization (GP) (Fig. 1c) as a measure of the lipid chain order to determine the membrane state [15]. To determine the respective intensities we fit the spectral data by two lognormal functions as proposed by *Bacalum* et al. [16].

2. Materials and methods

2.1. Spectrum acquisition

Spectrum acquisition was performed by use of the Ocean optics QEPro spectrometer and an optical fiber connected to the custom-made temperature control setup that is depicted in Fig. 1a. 600 µl of sample suspension containing the membrane of interest were analyzed in the glass capillary embedded in an aluminum block. A stir bar prevented sedimentation and ensured a homogenous temperature distribution within the sample. The temperature was measured with a Pt100 sensor placed in the suspension and regulated in a range from −40 to 95 °C by a peltier element cooled by a water bath. Laurdan was excited at 360 nm by an ultraviolet LED with UV-bandpass. The emitted light was captured after an UV-band-stop-filter by an optical fiber without any focusing optical elements. Data points were taken in steps of 1 °C. The scan rate was 2 °C per minute.

2.2. Multilamellar phospholipid vesicles

Multilamellar phospholipid vesicles were prepared in glass bottles by drying Laurdan (Sigma-Aldrich Chemie GmbH, Munich, Germany) and lipids (Avanti Polar lipids, AL, USA) dissolved in chloroform under nitrogen flow followed by vacuum exposure for at least 60 min. Vesicle swelling in ultra-pure water was promoted by ultra-sonication 15 K above the melting transition of the respective lipid species. The final concentration of lipids and Laurdan were 1 mM and 10 µM.

2.3. HeLa cells and B35 cells

HeLa cells (ATCC® CCL-2™) and B35 cells (ATCC® CRL-2754™) were cultured in 25 cm^2 NuncTM cell culture flasks (ThermoFisher Scientific, MA, USA) at 37 °C in saturated atmosphere. The culture media were DMEM for HeLa cells and DMEM with high glucose content (Bio&SELL GmbH, Nürnberg, Germany) for B35 cells, both supplemented with 10% fetal bovine serum (FBS Superior) and 1% Pen/Strep (Biochrom GmbH, Berlin, Germany). Membranes were stained in culture medium after addition of Laurdan dissolved in DMSO (1 mg/ml) for 2 h at 37 °C. The final concentration of Laurdan and DMSO in the staining solution were 28 µM and 141 mM (11 mg/l). After the staining procedure the cells were rinsed three times with PBS buffer, trypsinated with 1 ml of 0,05% trypsin/EDTA (Biochrom GmbH, Berlin, Germany) and analyzed without further treatment.

2.4. Cholesterol depleted HeLa cells

Cholesterol depleted HeLa cells were prepared by addition of 5 mM Methyl-beta-cyclodextrin after staining and trypsinization in the above-described manner. After 1 h treatment time without stirring at 37 °C the suspension was centrifuged at 300*g* for 3 min and the supernatant was replaced by fresh PBS buffer. Before optical analysis the cells pellet was resuspended by vortexing. In contrast to the temperature scan the cholesterol depletion kinetics were analyzed under steady stirring.

2.5. HeLa cell adaptation

HeLa cell adaptation was introduced by lowering the culture temperature by 1 K per week. After reaching the final temperature of 30 °C

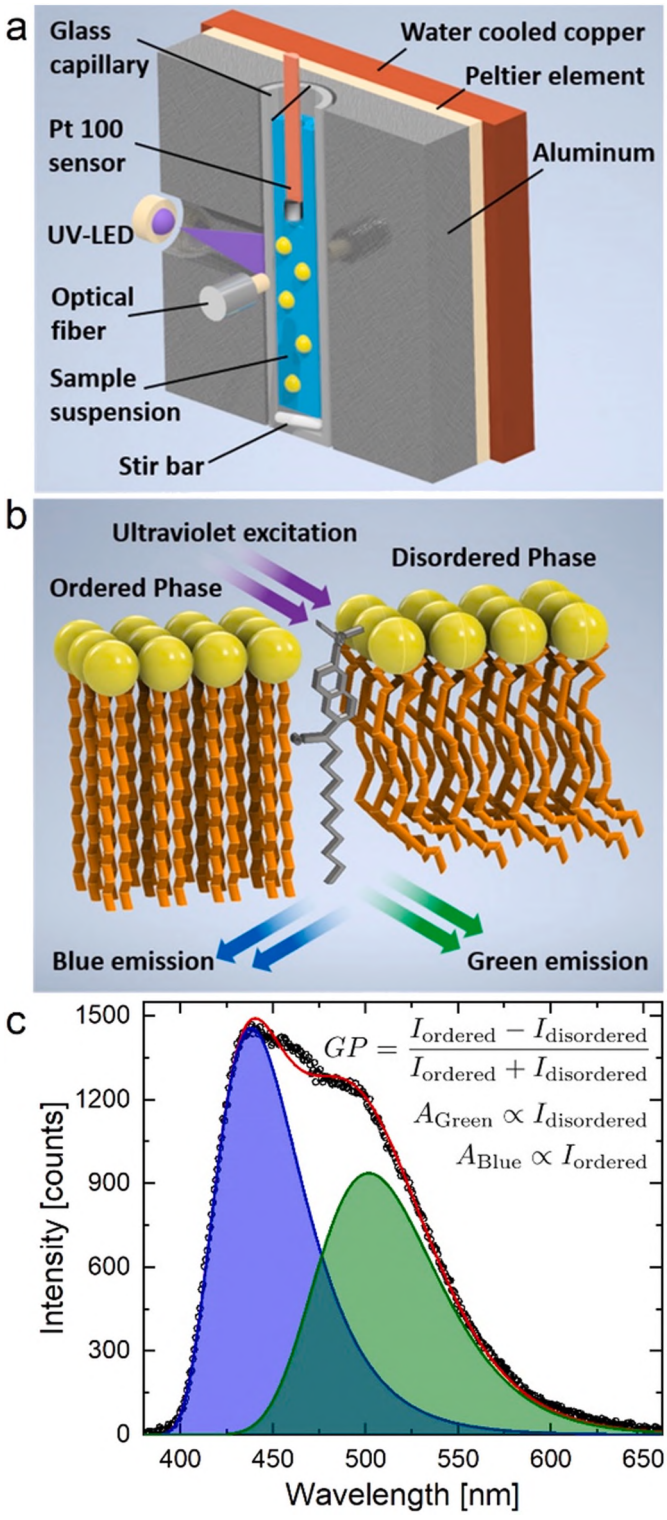

Fig. 1. Experimental setup and data analysis. **a** For optical analysis the sample suspension is placed in a glass capillary that can be temperature controlled in a broad temperature range. The fluorescence emission is recorded by a spectrometer attached to an optical fiber. **b** The membrane embedded dye Laurdan allows for determination of the phase state of lipid membrane samples due to its polarity sensitive emission spectrum. **c** The fluorescence intensities originating from ordered/disordered lipid domains are determined by data fitting to calculate the generalized polarization as measure for the membrane phase state.

no cell division took place for about one month. Over a period of further 3 months, the cell's growth rate increased up to one division per week. After the adaptation phase, the cells were analyzed as described above.

2.6. B35 cells with octanol

B35 cells with octanol were prepared by using a trypsin solution with 1 mM octanol for trypsinization after staining. The sample was directly afterwards analyzed.

2.7. Differentiated B35 cells

Differentiated B35 cells were obtained after incubation of a confluently grown cell flask in a 2 mM DcAMP culture medium solution at 37 °C for 24 h.

2.8. Red blood cell ghosts

Red blood cell ghosts were prepared following the procedure of Himbert et al. [17]: 300 µl of venous blood (friendly supplied by University Hospital Augsburg) were diluted with 1700 µl PBS buffer followed by centrifugation for 3 min at 600*g* and subsequent removal of the supernatant. After repeating this washing procedure three times, the cells were ruptured by exposure to hypotonic buffer (1.6 ml PBS buffer and 48.4 ml ultra-pure water buffered with sodium hydroxide at pH 8) for 30 min in an ice bath. The sample was centrifuged at 18,000*g* for 30 min followed by buffer exchange. The following three washing steps were performed at 18000 g for 15 min. The ghosts were stained in the hypotonic buffer containing 28 µM Laurdan and 141 mM DMSO for 2 h at 37 °C. Then the sample was again centrifuged at 18,000*g* for 15 min and the staining solution was replaced by buffer adjusted with monopotassium phosphate and disodium phosphate adjusted to the pH values 5,6 and 7. This solution was analyzed after resuspending the ghosts by vortexing.

2.9. Multilamellar HeLa and B35 membrane vesicles

Multilamellar HeLa and B35 membrane vesicles were prepared by following the lipid extraction protocol of Folch et al. [18]. After trypsinization about 2mio cells were centrifuged at 300*g* for 3 min followed by supernatant removal. The pellet was transferred into 2 ml of a chloroform/methanol solution (2:1) and lyzed by sonication for 30 min at 70 °C. After addition of 400 µl ultra-pure water and vortexing for 30 s the solution was centrifuged at 100*g* for 15 min. The lower part of the resulting biphasic solution, containing mainly chloroform and lipids, was transferred into another glass vial and Laurdan dissolved in chloroform was added. After drying under nitrogen flow and vacuum exposure for at least 60 min the lipids were hydrated with 1 ml of PBS buffer and vesicle swelling was induced by ultra-sonication at 70 °C for 30 min. The final concentration of Laurdan was 10 µM. The lipid content can be estimated using the findings of Delgado et al. who measured for mouse embryonic fibroblasts that lipids account for 13% of 500 pg dry mass per cell [19]. If we use these values for our cell lines it leads to 130 pg of lipids per sample. With a rough guess for the mean molecular lipid weight of about 500 g/mol we estimate the final lipid concentration to be 260 µM.

Multilamellar HeLa vesicles with reduced oxygen exposure were prepared as described before but all solvents were degassed by nitrogen bubbling for at least 60 min. Furthermore, the extraction procedure was carried out in a glovebox under nitrogen atmosphere.

2.10. Statistics

The data points of the shown GP temperature scans of cellular membranes represent the mean value of three independent measurements. The error bars show the standard deviation or in case of the ΔGP curves the pooled standard deviations. We performed two tailed *t*-tests with four degrees of freedom to test for 5% statistical significance between GP values. The fit parameters of the Boltzmann sigmoid function were compared by two tailed *t*-tests on 5% statistical significance as well. The data of three independent sample downscans (130 data points per scan from 90 °C to −40 °C, 390 points in summary, 4 fit parameters and therefore 386 degrees of freedom) were approximated by one function. The number of degrees of freedom for comparison of two fit parameters were 772 for a scan from 90 °C to −40 °C.

3. Results and discussion

3.1. Calorimetric and optical analysis of phospholipid vesicles

First, we examined the possibility of measuring the phase state of synthetic lipid membranes optically in a temperature range from T = -40 °C to T = 95 °C. Therefore, we compared calorimetric data of five different vesicle suspensions with temperature scans of the GP value and its derivative with respect to temperature (Fig. 2). These measurements were performed in a temperature controlled glass capillary that is schematically shown in Fig. 1a. Our data proves that we are in case of 13:0PC, 14:0PC, 15:0PC and 15:0PC with 10% cholesterol not only able to detect the correct location of phase transitions in lipid membranes but also peak width and height show similar behavior in both data sets. According to literature DOPC shows a phase transition as measured by DSC in a temperature range from −16.5 °C to −21 °C [20–22]. Thus, it is suited to examine if there are still Laurdan dynamics in membranes surrounded by frozen water. Fig. 2 show that even though we see a drop in the derivate of the GP curve at T = 0 °C (Fig. 2a inset) indicating that the GP value is somehow affected by water freezing it is still possible to detect the phase transition optically since our data shows a peak at T = -16.5 °C.

3.2. HeLa cell membrane state, adaptation and cholesterol depletion

In the following, we compare such phase state measurements on synthetic and biological membranes. For the latter we always analyzed the down scan since the GP changes stay reversible after the first heating (Supplementary Fig. 1a). The deviations between the first upscan and all following scans can be attributed to denaturation of proteins. Fig. 3 shows the temperature dependent Laurdan emission spectra of 14:0PC multilamellar vesicles (MLV) and HeLa cell membranes. In both cases close to T = 25 °C the emission shifts from blue to green indicating a change from an ordered to a disordered state. The difference lies in the steepness of the transition indicating differences in cooperativity. The peak in the derivative with respect to temperature of the 14:0PC MLV sample is 20 times higher than the one of the HeLa cells. The small peak height meaning low cooperativity might be the reason why we were not able to measure the transition by DSC and may be attributed amongst others to the variability of cell membranes and high cholesterol content in eukaryotic cell membranes. When we investigated phase state changes during the trypsinization process of HeLa cells, we found a variation of GP values at constant temperature of $\Delta GP \approx 0.02$ (Supplementary Fig. 1 b, c). During this measurement, about 100 cells were in the focus range of the spectrometer. Therefore, one can conclude that the variability of single cells is even higher. This result is in good agreement with previous studies where GP distributions even within single cell membranes were found [23]. Accordingly, the presented temperature scans including millions of cells in suspension are a sum of various slightly different melting events resulting in a broad transition. As shown in Fig. 2, cholesterol reduces the cooperativity in synthetic membranes making transitions harder to detect. In contrast to HeLa cells bacteria are not able to synthesize cholesterol and show in consequence sharper transitions [24]. Taken together, this might be the reason why we could not measure a phase transition in HeLa membranes using DSC.

To examine the effect of cholesterol content on the phase state of

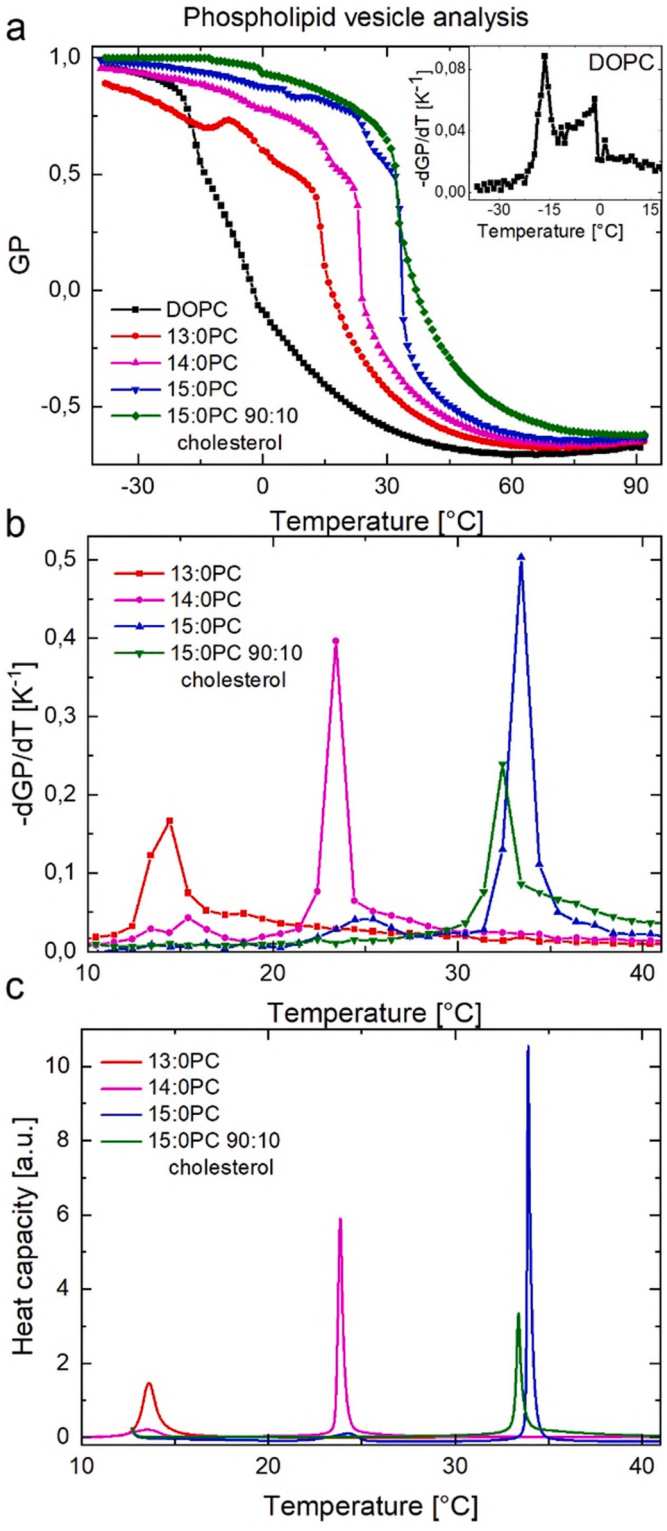

Fig. 2. Phospholipid vesicle analysis. **a** Temperature dependent generalized polarization of various phospholipid multilamellar vesicles measured during heating. The inset shows the derivative with respect to temperature of DOPC vesicles with a peak at T = -16.5 °C indicating the ordered/disordered phase transition. **b** Derivative with respect to temperature of various lipid vesicles showing the same ordered/disordered phase transitions as their heat capacity profiles measured by DSC in **c**.

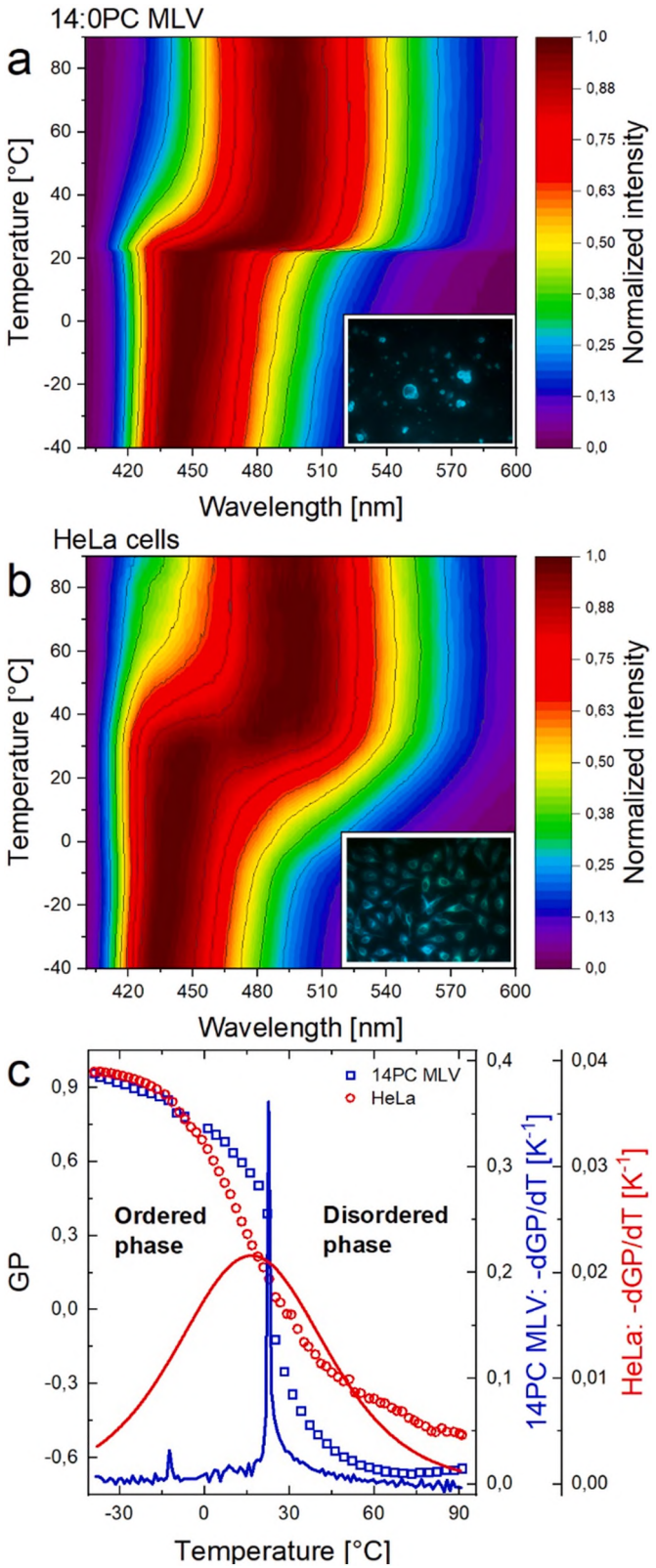

Fig. 3. Comparison of phospholipid vesicles and HeLa cell membranes. **a, b** Normalized emission spectra of 14:0PC multilamellar vesicles/HeLa cells as a function of temperature and fluorescence microscopy images of the samples (field of view about 420 × 320 μm^2). **c** GP of 14:0PC multilamellar vesicles/HeLa cells as a function of temperature and their corresponding derivatives after temperature at two differently scaled axes.

HeLa membranes we depleted the membranes by exposure to methyl-beta-cyclodextrin. Fig. 4 shows GP as function of temperature for wild type, growth temperature adapted, cholesterol depleted HeLa cells and lipid extracts from these cells. Fig. 4a shows that cholesterol depletion caused a shift of the GP curve especially at around $T = 30$ °C towards lower values corresponding to increased disorder in the membrane. Recent studies of Pérez et al. suggest that this change could be attributed to the reduced water repulsion due to cholesterol [25]. Consequently, the transition becomes steeper and the cooperativity determined by the steepness of a Boltzmann sigmoid fit function at the inflection point increases by 23%, as shown in Fig. 4b. The other fit parameters namely the span and inflection point corresponding to melting enthalpy ΔH and melting Temperature T_m are affected as well and decreased by $\Delta H/H \approx -4\%$ and $\Delta T_m \approx -2.4$ K. The inset in Fig. 4a shows the GP values in a

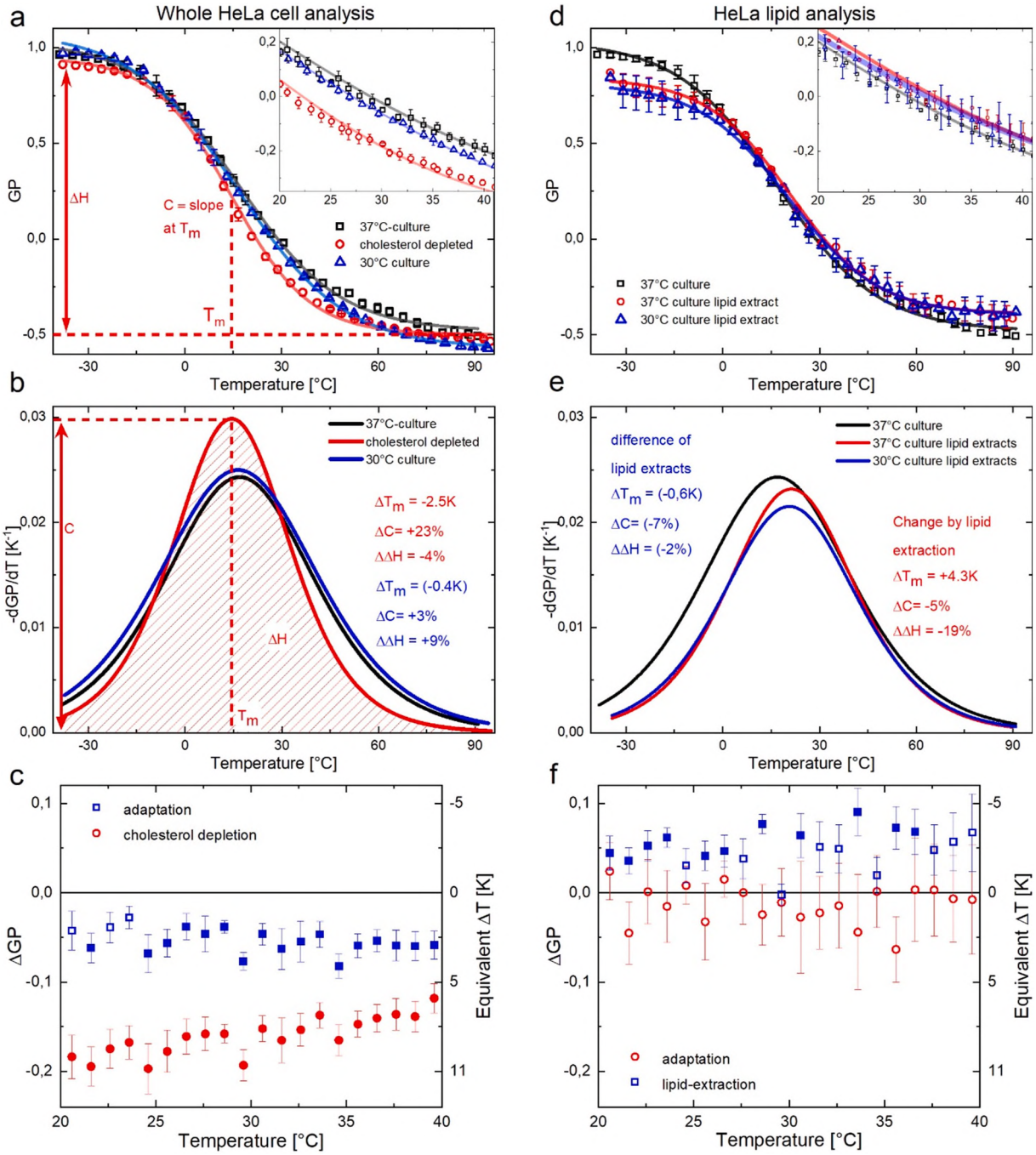

Fig. 4. Phase state analysis of HeLa cell membranes and their lipid extracts under varying conditions. **a,d** Temperature dependent GP values of untreated, cholesterol depleted and low temperature (30 °C) adapted HeLa cell membranes and their lipid extracts. Each data point represents the mean value with standard deviation of at least 3 independent samples. For visibility, only every fourth point is shown. The data is approximated by a Boltzmann sigmoid function, which allows for determination of the point of inflection or Tm, its steepness as a measure for cooperativity C and the span corresponding to a melting enthalpy ΔH. The inset shows GP values in a physiologically relevant temperature interval and the 95% confidence intervals of the according fit functions. **b,e** Derivatives after temperature of GP graphs pictured in A and D. The changes of melting temperature ΔTm, cooperativity ΔC and melting enthalpy ΔΔH due to adaptation, cholesterol depletion and lipid extraction are calculated by comparison of the Boltzmann sigmoid fit parameters. **c,f** Temperature dependent GP changes induced by adaptation, cholesterol depletion and lipid extraction. Data points with a *P*-value larger than 5% are represented by hollow symbols. The equivalent temperature changes are calculated by the use of a linear approximation of untreated HeLa cells in the temperature regime from 20 °C to 40 °C.

physiological temperature regime. A linear approximation of GP as function of temperature for the reference HeLa cells in a temperature regime from 20 °C to 40 °C gives a slope of 5.3 K per 0.1 GP. Using this slope, we can convert GP changes into equivalent temperature changes ΔT, as this might be more intuitive than bare changes in membrane (dis) order. Fig. 4c shows these equivalent temperature changes ΔT. Following this concept, the cholesterol depletion induces a decrease in lipid order that corresponds to an increase in temperature of ΔT = +7 K to ΔT = +11 K (Fig. 4c).

Heimburg et al. measured phase transitions in the lysate of *Escherichia coli* bacteria, which contain no cholesterol in their membranes by DSC. They found a transition slightly below the culture temperature. Furthermore, this transition shifted towards lower temperatures after culture below physiological temperatures [26]. Similar adaptation effects were observed in giant plasma membrane vesicles of zebrafish cell lines [27]. Inspired by these findings we decreased the culture temperature of HeLa cells from $T = 37$ °C to $T = 30$ °C (temperature ramp -1 K/week) and kept it at $T = 30$ °C over a period of about 5 months before we measured membrane order as function of temperature (Fig. 4a, "30 °C culture"). In accordance with bacteria data the GP values of these eukaryotic cells decreased by $\Delta T = 2.5$ K temperature equivalent (Fig. 4c) due to adaptation meaning that the cells compensate the increased order caused by the lower temperature by adjusting the membrane composition to reduce order again. The position of the derivative peak is almost not affected but a 3% increase of slope C as measure for the cooperativity is seen (Fig. 4b). To examine whether the GP change is caused by alteration of lipids or protein we applied the Folch method to split a cell lysate into a water soluble part containing most of the proteins and an unpolar part with all the lipid molecules of the cells [18]. The latter was dried and rehydrated to obtain HeLa cell membrane multilamellar vesicles. The comparison of the temperature dependent GP values of regular HeLa cells with their lipid extracts is shown in Fig. 4d. The difference between those samples can be attributed on the one hand to the presence of proteins within the lipid membrane. On the other hand polyunsaturated lipids are chemically labile and oxidative lipid breakdown can influence the membrane phase state as well [28,29]. We checked whether oxygen exposure during the lipid extraction procedure influenced the measured GP-profiles but could not observe any effect (see Supplementary Fig. 2). Furthermore, asymmetries within the intact cell membrane affect lipid phase transitions too and are lost after extraction and rehydration [30,31]. The melting transition of the lipid extract displayed in Fig. 4e is clearly shifted by 4.3 K towards higher temperatures. Therefore, the lipid extraction causes a melting point depression. This trend might be even more pronounced considering that the lipid to probe ratio was rather low (26:1) compared to vesicle experiments (100:1) which causes membranes to be more fluid as measurements on 15:0PC vesicles and the analysis of the membrane staining process show (Supplementary Fig. S1 e, f). Furthermore, membranes with proteins show broader transitions with 5% higher cooperativity and 19% higher melting enthalpy. The differences in GP shown in Fig. 4f show the same trend as the GP derivatives: Membranes without proteins display GP values that correspond to temperatures changes of down to -5 K.

Even though it is difficult to identify the process that causes the phase state changes during lipid extraction, the comparison of extracts of the 30 °C and 37 °C HeLa cultures should answer the question whether mainly the lipid composition is altered during the adaptation process to colder culture temperatures or not since none of those samples contain significant amounts of protein. Both temperature scans are shown in Fig. 4d. The according melting transitions in Fig. 4e display no statistically significant change but again a trend of melting point reduction is visible as seen for the whole cell analysis in Fig. 4b. The same holds for the ΔGP values in Fig. 4f that do not differ from 0 with a p value lower than 0.05 meaning that the GP of the lipid extracts in the physiological temperature regime is not changed by adaptation as pronounced as for the whole cells. Therefore, we conclude that the alteration of the lipid composition during adaptation to lower culture temperatures plays a minor role compared to changes in protein composition. Our results are in good agreement with the findings of Heimburg et al. who observed phase state changes in *E. coli* bacteria membranes during adaptation as well [26].

3.3. Neuroblastoma cell membrane after differentiation and anaesthetic exposure

To contribute to the discussion whether phase transitions in biological membranes play a role in the signaling mechanism of nerve cells [3,32,33] we analyzed B35 neuroblastoma cells and how their membrane order-disorder-transition is affected by differentiation and exposure to an anaesthetic. Applying the same concept as shown in Fig. 4 for HeLa cells, Fig. 5 shows GP as function of temperature, it's derivative with respect to temperature in absence and presence of octanol and differentiated as well as undifferentiated. It is known for lipid vesicles that the phase transition temperature is lowered after incorporation of an anaesthetic meaning that the disordered phase expands [34]. In Fig. 5a we see that the same applies for B35 Neuroblastoma membranes when they get exposed to 1 mM octanol. We see a GP change equivalent to about ΔT = -2 K to ΔT = -5 K left shift in the physiological regime (Fig. 3c) and a global peak shift of ΔT = - 3 K (Fig. 3b). While the melting enthalpy of the transition is almost not affected by octanol addition, the cooperativity is decreased by 3%. The effect of anaesthetic exposure was examined by the use of undifferentiated B35 cells, which do not form neurites. Investigations on HeLa cells during the trypsinization process showed that the morphological change from adherent to suspended is accompanied by a change of the membrane phase state (Supplementary Fig. 1b). Therefore, we treated B35 neuroblastoma cells for 24 h with Dibutyryl-adenosine 3′,5′-cyclic monophosphate sodium salt (DcAMP) to promote neurite outgrowth (Supplementary Fig. 1d) and examined the phase state of these differentiated cells. The measured GP change after differentiation corresponds to a shift of up to ΔT = - 4 K towards lower temperatures (Fig. 5c) accompanied by a movement of the melting transition by $\Delta T_m = -1.4$ K in the same direction. Furthermore, the melting enthalpy and cooperativity are reduced by differentiation (Fig. 5b). We performed measurements on the lipid extracts of differentiated and undifferentiated B35 cells and find again by comparison of whole cell analysis and lipid extracts that the transition of the lipid extracts is narrower and shifted towards higher temperatures as seen for HeLa cells meaning that proteins cause a melting point depression in cell membranes (Figs. 4e and 5e). Fig. 5b shows the GP profiles of lipid extracts of differentiated and undifferentiated cells. A comparison of these samples should reveal membrane changes during differentiation that can be attributed exclusively to an alteration of the lipid composition. A small positive shift of $\Delta T = 0.9$ K of the melting transition can be seen in Fig. 5e. This result differs from the one obtained from the whole cell analysis and could indicate that the membrane phase state changes during differentiation due to alteration of both lipid and protein composition.

3.4. Red blood cell ghosts at different pH levels

To stress the multidimensionality of membrane phase diagrams, in the following we analyze order disorder transitions in red blood cells that are sensitive for pH changes. It is known that red blood cells (RBC) show protonation dependent membrane properties e.g. permeability [35] that can be understood by charge effects in lipid head groups. RBC are exposed to varying pH levels in the human body depending on whether they are located in healthy tissue or in inflamed regions, were the pH can drop down to about pH 6 [36]. We here study red blood cell ghosts as the absorbance of hemoglobin interferes with the Laurdan fluorescence signal. Fig. 6a shows the temperature dependent GP of RBC at the pH levels 5,6 and 7. The GP curve shifts for pH 6 slightly, for pH 5 more pronounced towards higher temperatures meaning an expansion

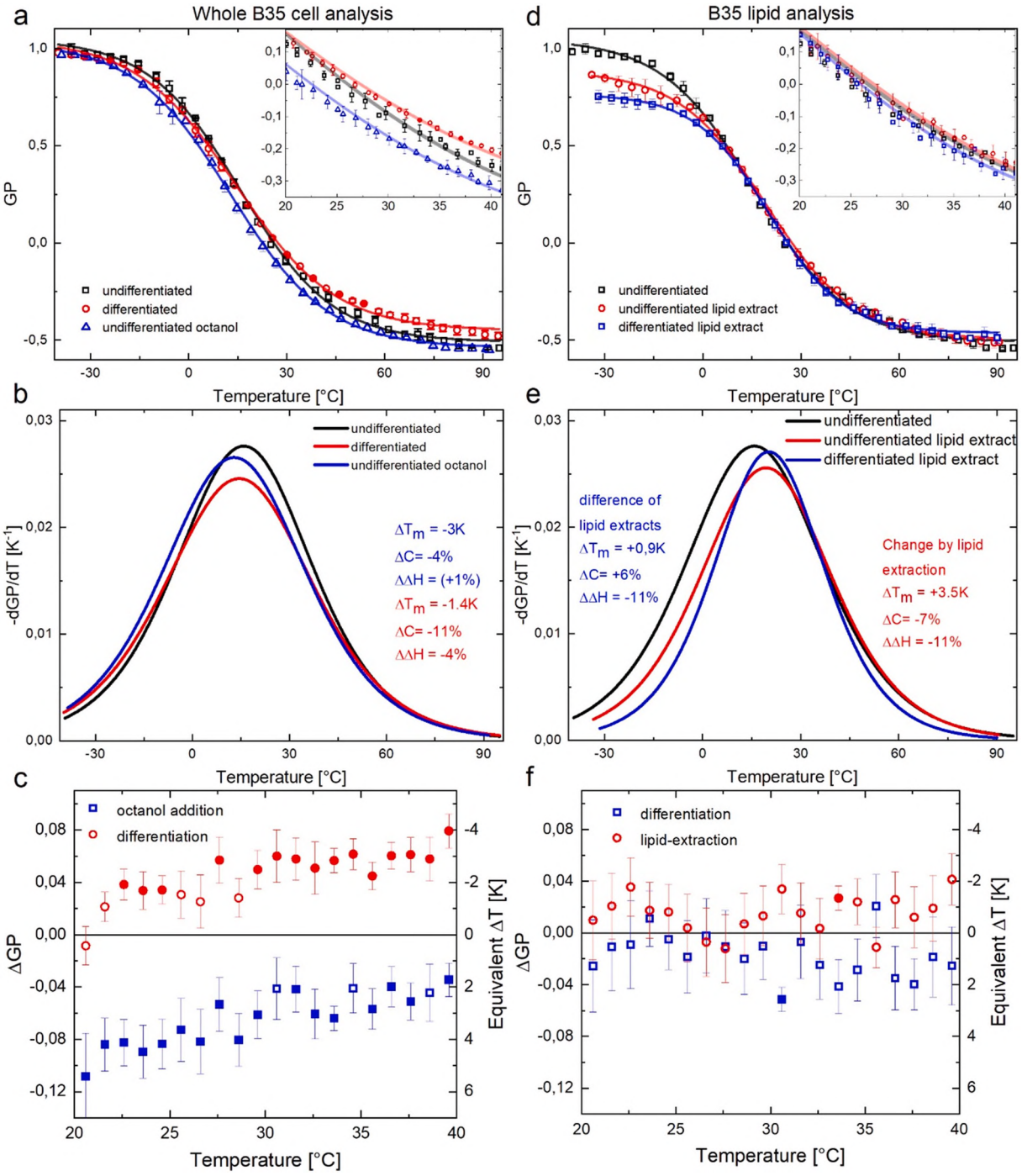

Fig. 5. Phase state analysis of B35 Neuroblastoma cell membranes and their lipid extracts under varying conditions. **a,d** Temperature dependent GP values of untreated, differentiated and octanol (1 mM) exposed cell membranes and their lipid extracts. Data point representation, error bars and fit values in **a-f** are treated as described in Fig. 4.

of the ordered phase due to protonation shown in the inset of Fig. 6a for a constant temperature of $T = 37$ °C. Therefore, RBC membranes react to pH changes as it is known for synthetic membranes containing charged headgroups [9]. The transition calculated by data fitting and building the derivative with respect to temperature in Fig. 6b shows the same behavior. While there is almost no change from pH 7 to pH 6 the melting temperature T_m shifts at pH 5 by $\Delta T_m = +1.5$ K to the right compared to pH 7. Cooperativity and melting enthalpy are reduced by protonation. The pH dependent shift in the physiological temperature regime depicted in the upper inset again can be translated in a ΔGP with corresponding equivalent temperature change ΔT (Fig. 6c). For pH 7 lipid order is increased as it would be after a temperature reduction of $\Delta T = -4$ K to $\Delta T = -6$ K.

4. Conclusions

In summary we have not only shown the presence of broad order-disorder phase transitions in biological membranes but also that they are affected by cholesterol, anaesthetic, and pH in the same way as it is known for sharp transitions in synthetic membranes. Even though the transition itself is not visible in the physiological temperature regime where lipid order changes only linearly with temperature, the

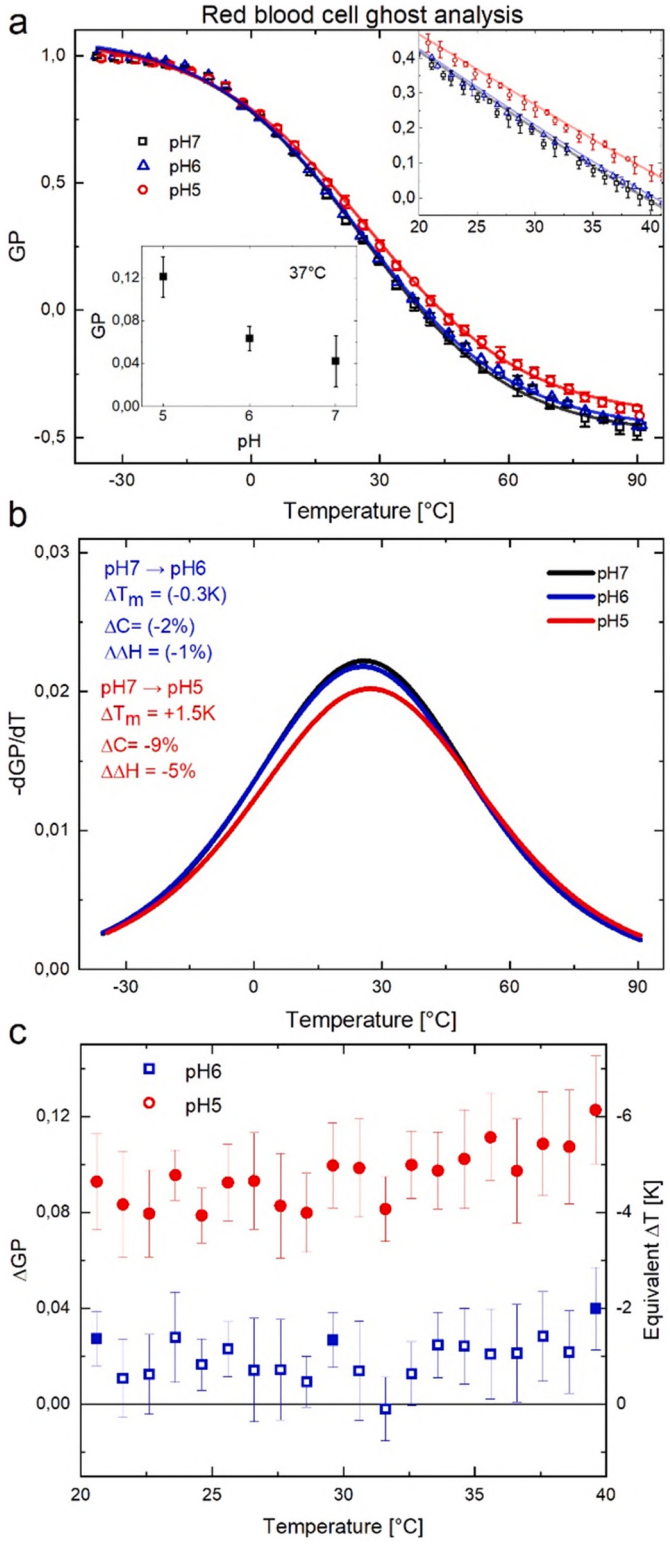

Fig. 6. Phase state analysis of red blood cell ghosts under varying pH levels. **a** Temperature dependent GP values of red blood cell ghosts at pH 7, pH 6 and pH 5. Data point representation, error bars and fit values in **a-c** are treated as described in Fig. 4. (For interpretation of the references to colour in this figure legend, the reader is referred to the web version of this article.)

knowledge about the underlying physics of this effect allows for prediction how membrane order reacts to environmental changes. This approach could prove itself useful since our findings that lipid order is affected by adaptation processes and morphological changes during differentiation or trypsinization suggest that cellular functionality is indeed connected to the membrane state. Exciting studies based on these results may include but are not limited to in-depth studies on substance and signal transport across and along the membrane.

CRediT authorship contribution statement

N.F. and C.W. designed research; N.F. and C.W. performed research; N.F. analyzed data and implemented experimental tools; N.F. and C.W. wrote the paper.

Declaration of competing interest

The authors declare the following financial interests/personal relationships which may be considered as potential competing interests: Nicolas Faerber reports financial support was provided by Joachim Herz Foundation.

Data availability

All data that support our findings are available from the corresponding authors upon reasonable request. There are no restrictions on data availability.

Acknowledgements

The authors thank Prof. Dr. Matthias Schneider, Simon Fabiunke and Achim Wixforth for fruitful discussions. The authors thank the Center for NanoScience, Ludwig-Maximilians-Universität München (CeNS) and the Augsburg Centre for Innovative Technologies (ACIT) for funding. C.W. would like to acknowledge funding for the project "Physical and functional interaction mechanisms at cell membranes and vessel walls" by the University of Augsburg. N.F. would like to thank the Joachim Herz foundation. Furthermore, the authors thank Dr. Stefanie Grützner for providing blood samples and Sebastian Pentz for technical assistance.

Appendix A. Supplementary data

Supplementary data to this article can be found online at https://doi.org/10.1016/j.bbamem.2021.183794.

References

[1] A. Blicher, K. Wodzinska, M. Fidorra, M. Winterhalter, T. Heimburg, The temperature dependence of lipid membrane permeability, its quantized nature, and the influence of anesthetics, Biophys. J. 96 (2009) 4581–4591, https://doi.org/10.1016/j.bpj.2009.01.062.

[2] H. Ebel, P. Grabitz, T. Heimburg, Enthalpy and volume changes in lipid membranes. I: the proportionality of heat and volume changes in the lipid melting transition and its implication for the elastic constants, J. Phys. Chem. B 105 (2001) 7353–7360, https://doi.org/10.1021/jp010515s.

[3] T. Heimburg, A.D. Jackson, On soliton propagation in biomembranes and nerves, Proc. Natl. Acad. Sci. U. S. A. 102 (2005) 9790–9795, https://doi.org/10.1073/pnas.0503823102.

[4] F.G. Strobl, F. Seitz, C. Westerhausen, A. Reller, A.A. Torrano, C. Bräuchle, et al., Intake of silica nanoparticles by giant lipid vesicles: influence of particle size and thermodynamic membrane state, Beilstein J. Nanotechnol. 5 (2014) 2468–2478, https://doi.org/10.3762/bjnano.5.256.

[5] T. Parasassi, E.K. Krasnowska, L. Bagatolli, E. Gratton, in: Laurdan and Prodan as Polarity-sensitive Fluorescent Membrane Probes 8, 1998, pp. 365–373.

[6] C. Scomparin, S. Lecuyer, M. Ferreira, T. Charitat, B. Tinland, Diffusion in supported lipid bilayers: influence of substrate and preparation technique on the internal dynamics, Eur. Phys. J. E 28 (2009) 211–220, https://doi.org/10.1140/epje/i2008-10407-3.

[7] R.A. Böckmann, A. Hac, T. Heimburg, H. Grubmüller, Effect of sodium chloride on a lipid bilayer, Biophys. J. 85 (2003) 1647–1655, https://doi.org/10.1016/S0006-3495(03)74594-9.

[8] T. Heimburg, The capacitance and electromechanical coupling of lipid membranes close to transitions: the effect of electrostriction, Biophys. J. 103 (2012) 918–929, https://doi.org/10.1016/j.bpj.2012.07.010.
[9] H. Trauble, H. Eibl, Electrostatic effects on lipid phase transitions: membrane structure and ionic environment, Proc. Natl. Acad. Sci. U. S. A. 71 (1974) 214–219, https://doi.org/10.1073/pnas.71.1.214.
[10] J.V. Busto, A.B. García-Arribas, J. Sot, A. Torrecillas, J.C. Gómez-Fernández, F. M. Goñi, et al., Lamellar gel (Lβ) phases of ternary lipid composition containing ceramide and cholesterol, Biophys. J. 106 (2014) 621–630, https://doi.org/10.1016/j.bpj.2013.12.021.
[11] R.N. McElhaney, Differential scanning calorimetric studies of lipid-protein interactions in model membrane systems, Biochim. Biophys. Acta Rev. Biomembr. 864 (1986) 361–421, https://doi.org/10.1016/0304-4157(86)90004-3.
[12] T. Parasassi, F. Conti, E. Gratton, Time-resolved fluorescence emission spectra of laurdan in phospholipid vesicles by multifrequency phase and modulation fluorometry, Cell. Mol. Biol. 32 (1986) 103–108.
[13] T. Parasassi, E. Gratton, Packing of phospholipid vesicles studied by oxygen quenching of laurdan fluorescence, J. Fluoresc. 2 (1992) 167–174, https://doi.org/10.1007/BF00866931.
[14] S.S.W. Leung, J. Brewer, L.A. Bagatolli, J.L. Thewalt, Measuring molecular order for lipid membrane phase studies: linear relationship between laurdan generalized polarization and deuterium NMR order parameter, Biochim. Biophys. Acta Biomembr. 1861 (2019), 183053, https://doi.org/10.1016/j.bbamem.2019.183053.
[15] T. Parasassi, G. De Stasio, G. Ravagnan, R.M. Rusch, E. Gratton, Quantitation of lipid phases in phospholipid vesicles by the generalized polarization of laurdan fluorescence, Biophys. J. 60 (1991) 179–189.
[16] M. Bacalum, B. Zorila, M. Radu, Fluorescence spectra decomposition by asymmetric functions: laurdan spectrum revisited, Anal. Biochem. 440 (2013) 123–129, https://doi.org/10.1016/j.ab.2013.05.031.
[17] S. Himbert, R.J. Alsop, M. Rose, L. Hertz, A. Dhaliwal, J.M. Moran-Mirabal, The molecular structure of human red blood cell membranes from highly oriented, solid supported multi-lamellar membranes, Sci. Rep. 7 (2017) 1–14, https://doi.org/10.1038/srep39661.
[18] J. Folch, M. Lees, G.H. Sloane Stanley, A simple method for the isolation and purification of total lipides from animal tissues, J. Biol. Chem. 226 (1957) 497–509.
[19] F. Feijó Delgado, N. Cermak, V.C. Hecht, S. Son, Y. Li, S.M. Knudsen, Intracellular water exchange for measuring the dry mass, water mass and changes in chemical composition of living cells, PLoS One (2013) 8, https://doi.org/10.1371/journal.pone.0067590.
[20] P.G. Barton, F.D. Gunstone, Hydrocarbon chain packing and molecular motion in phospholipid bilayers formed from unsaturated lecithins, J. Biol. Chem. 250 (1975) 4470–4476.
[21] P.J. Davis, K.M.W. Keough, Differential scanning calorimetric studies of aqueous dispersions of mixtures of cholesterol with some mixed-acid and single-acid phosphatidylcholines, Biochemistry 22 (1983) 6334–6340, https://doi.org/10.1021/bi00295a045.
[22] R.N. Lewis, B.D. Sykes, R.N. McElhaney, Thermotropic phase behavior of model membranes composed of phosphatidylcholines containing cis-monounsaturated acyl chain homologues of oleic acid: differential scanning calorimetric and31P NMR spectroscopic studies, Biochemistry 27 (1988) 880–887, https://doi.org/10.1021/bi00403a007.
[23] T. Parasassi, E. Gratton, W.M. Yu, P. Wilson, M. Levi, Two-photon fluorescence microscopy of laurdan generalized polarization domains in model and natural membranes, Biophys. J. 72 (1997) 2413–2429, https://doi.org/10.1016/S0006-3495(97)78887-8.
[24] Z. Huang, E. London, Cholesterol lipids and cholesterol-containing lipid rafts in bacteria, Chem. Phys. Lipids 199 (2016) 11–16, https://doi.org/10.1016/j.chemphyslip.2016.03.002.
[25] H.A. Pérez, A. Disalvo, M.de los Á. Frías, Effect of cholesterol on the surface polarity and hydration of lipid interphases as measured by Laurdan fluorescence: new insights, Colloids Surf. B: Biointerfaces (2019) 178.
[26] T. Mužić, F. Tounsi, S.B. Madsen, D. Pollakowski, M. Konrad, T. Heimburg, Melting transitions in biomembranes, Biochim. Biophys. Acta Biomembr. 1861 (2019), 183026, https://doi.org/10.1016/j.bbamem.2019.07.014.
[27] M. Burns, K. Wisser, J. Wu, I. Levental, S.L. Veatch, Miscibility transition temperature scales with growth temperature in a zebrafish cell line, Biophys. J. 113 (2017) 1212–1222, https://doi.org/10.1016/j.bpj.2017.04.052.
[28] J. Zhao, J. Wu, H. Shao, F. Kong, N. Jain, G. Hunt, et al., Phase studies of model biomembranes: macroscopic coexistence of Lα + Lβ, with light-induced coexistence of Lα + lo phases, Biochim. Biophys. Acta Biomembr. 1768 (2007) 2777–2786, https://doi.org/10.1016/j.bbamem.2007.07.009.
[29] A.G. Ayuyan, F.S. Cohen, Lipid peroxides promote large rafts: effects of excitation of probes in fluorescence microscopy and electrochemical reactions during vesicle formation, Biophys. J. 91 (2006) 2172–2183, https://doi.org/10.1529/biophysj.106.087387.
[30] M.D. Collins, S.L. Keller, Tuning lipid mixtures to induce or suppress domain formation across leaflets of unsupported asymmetric bilayers, Proc. Natl. Acad. Sci. U. S. A. 105 (2008) 124–128, https://doi.org/10.1073/pnas.0702970105.
[31] A.J. Wagner, S. Loew, S. May, Influence of monolayer-monolayer coupling on the phase behavior of a fluid lipid bilayer, Biophys. J. 93 (2007) 4268–4277, https://doi.org/10.1529/biophysj.107.115675.
[32] B. Fichtl, S. Shrivastava, M.F. Schneider, Protons at the speed of sound: predicting specific biological signaling from physics, Sci. Rep. 6 (2016) 1–9, https://doi.org/10.1038/srep22874.
[33] B. Fichtl, I. Silman, M.F. Schneider, On the physical basis of biological signaling by Interface pulses, Langmuir 34 (2018) 4914–4919, https://doi.org/10.1021/acs.langmuir.7b01613.
[34] T. Heimburg, A.D. Jackson, The thermodynamics of general anesthesia, Biophys. J. 92 (2007) 3159–3165, https://doi.org/10.1529/biophysj.106.099754.
[35] R.J. Labotka, A. Omachi, The pH dependence of red cell membrane transport of titratable anions studied by NMR spectroscopy, J. Biol. Chem. 263 (1988) 1166–1173, https://doi.org/10.1016/s0021-9258(19)57281-7.
[36] S. Buchegger, A. Kamenac, S. Fuchs, R. Herrmann, P. Houdek, C. Gorzelanny, et al., Smart antimicrobial efficacy employing pH-sensitive ZnO-doped diamond-like carbon coatings, Sci. Rep. 9 (2019) 1–10, https://doi.org/10.1038/s41598-019-53521-7.